Electrically-driven control of nanoscale chemical changes in amorphous complex oxide memristive devices

Wilson Román Acevedo[1], Myriam H. Aguirre[2,3,4], Diego Rubi[1]

[1] *Instituto de Nanociencia y Nanotecnología (INN), CONICET-CNEA, Gral. Paz 1499, 1650 San Martín, Argentina*

[2] *Instituto de Nanociencia y Materiales de Aragón (INMA-CSIC), Campus Rio Ebro C/Mariano Esquillor s/n, 50018 Zaragoza, Spain*

[3] *Dpto. de Física de la Materia Condensada, Universidad de Zaragoza, Pedro Cerbuna 12, 50009 Zaragoza, Spain*

[4] *Laboratorio de Microscopías Avanzadas, Edificio I+D, Campus Rio Ebro C/Mariano Esquillor s/n, 50018 Zaragoza, Spain**

Abstract

Our study demonstrates that strong cationic segregation can occur in amorphous complex oxide memristors during electrical operation. With the help of analytic techniques, we observed that switching the electrical stimulation from voltage to current significantly prevents structural changes and cation segregation at the nanoscale, improving also the device cycle-to-cycle variability. These findings could contribute to the design of more reliable oxide-based memristors and underscore the crucial role of the type of electrical stimulation applied to these devices.

I. INTRODUCTION

Memristive systems are capacitor-like micro or nanostructures able to change their electrical resistance -usually in a non-volatile way- upon the application of electrical stimulation [1]. Initially, the technological importance of memristors was mostly linked to the possibility of developing Resistive Random Access Memories [2]; however, in the past few years, their ability to mimic the (analog) behavior of biological synapses triggered a great deal of research as they are thought to constitute one of the key building for the development of neuromorphic computing [3], intended to outperform standard Von-Neumann computers in data intensive tasks. At the moment, several proof-of-concept neuromorphic devices based on memristors have been developed and tested [4–6].

Memristive mechanisms usually rely on the reversible electromigration at the nanoscale of charged defects, leading to resistance changes in the device. In the particular case of insulating oxides, these defects are usually charged oxygen vacancies [7], which can form conducting nanofilaments that bridge both metallic electrodes [8]. On the other hand, oxygen vacancy dynamics can modulate the metal/oxide resistance via Schottky-barrier height modulation [1] or redox-reaction [9], leading to an area-distributed memristive effect.

Despite the mechanism of electrochemical metalization, where metallic ions coming from Ag or Cu electrodes form a conducting filament [10, 11], the possibility of chemical changes linked to cation electromigration has been less studied in oxide-based memristors [12, 13]. These changes, which can be self-accelerated by local Joule heating and should strongly depend on the specific protocol of external stimulation, might produce drastic effects in

* diego.rubi@gmail.com

the composition, nanostructure and, therefore, the memristive performance of oxide-based devices. The obtention of local information at the nanoscale [14] is essential to achieve a deep understanding and, thefore, control of the memsristive response of these devices.

It was previously shown in manganite-based devices that the memristive response strongly depends on the type of stimulation; for instance, the use of voltage stimulation produced a two-level memristive response with high cycle-to-cycle variations, while the use of current stimulation allowed the stabilization of a third resistance level [15, 16], together with an improved cycle-to-cycle variation and endurance. This difference can be rationalized in terms of the limited power injection during the SET process (high to low resistance transition) for the case of current stimulation, that limits self-heating effects and the concomitant nanostructural and chemical changes. For current stimulation, the electrical power is given by $P = I^2R$, with the power remaining self-limited for the SET transition. For the case of voltage stimulation, the electrical power is given by $P = V^2/R$ and the SET transition is linked to a power peak, even if a compliance current is used (we recall that electronic sources usually have a limited time response that can't avoid an unwanted power overshoot in a time-window of the order of ms, necessary to stabilize the compliance current).

In the present paper we study the chemical changes at the nanoscale on devices based amorphous thin films of the perovskite $La_{0.5}Sr_{0.5}Mn_{0.5}Co_{0.5}O_3$ (LSMCO) under different electrical stimulation. This system presents, in its crystalline form, the existence of both oxidized an reduced phases, which different conductivities, linked via a topotactic redox transition [17], which can be triggered electrically. When sandwiched between Nb:$SrTiO_3$ (n-type material) and Pt electrodes, crystalline LSMCO (p-type) presents a memristive effect concomitant with a strong memcapacitive one [18, 19]. The origin of this behavior relies on the formation of a switchable n-p diode, where the oxidation and reduction of LSMCO strongly changes the balance between n- and p-carriers at the interface which, controls the depletion layer and thus the interface capacitance and the electrical leakage. It was shown that the multi-mem behavior can be improved either by tuning the out-of-plane orientation, the type of electrical stimulation [19] and by incorporating dopants such as Ce [20], which enhance the perovskite reducibility by producing a steric effect that enlarges the perovskite unit cell. A similar enhancement of the reducibility was shown by controlling the unit cell deformation using substrates with different lattice mismatch [21].

Here we address, instead, LSMCO films grown at (low) CMOS-compatible temperatures

leading to amorphous films. In these conditions, cations are not placed in well defined minima of the crystalline structure and therefore are more prone to migrate during memristive operation. Our results show that the use of voltage or current as electrical stimulation has a dramatic effect on the chemistry of the devices. In the latter case, chemical changes are minimized and this leads to a more stable memristive behavior, with a lower cycle-to-cycle variability. These results might contribute to the design of memristive devices with higher reliability and better suited to endure electrical operation without suffering nanostructural and chemical changes.

II. EXPERIMENTAL

LSMCO thin films were grown on NSTO single crystals by Pulsed Laser Deposition, using a Nd:YAG laser ($\lambda = 266$ nm) with a repetition rate of 10 Hz. The deposition temperature was set in 200 °C and the oxygen background pressure was 0.085 mbar. The film thickness, as determined from x-ray reflectivity, was ≈ 38.5 nm. X-ray Bragg-Brentano scans, displayed in Figure S1, show the only presence of reflections arising from the substrate, confirming the amorphous nature of the films. Top Pt electrodes (≈ 29 nm thick) were microfabricated by standard UV litography and magnetron sputtering. The device area was $\approx 2.4x10^4\ \mu m^2$. The bottom NSTO electrode was grounded and electrical bias was applied to the top Pt electrode, by using a Keithley 2612 Source Meter Unit (SMU). Contact was made using tungsten tips and a commercial probe-station. Memristive characterization consisted in dynamic current-voltage (IV) curves [22], where voltage (current) pulses of electrical stimulation, with varying amplitude and polarity according to the scheme depicted in the inset of Figure 1(b), were applied and current (voltage) was measured during the application of the pulses. In addition to the dynamic IV curves, we measured on the same run the so-called hysteresis switching loops (HLS) [22, 23], which allows tracking the evolution the remnant resistance immediately after the application of each write pulse. For that, a small reading pulse of voltage (current) is applied in between write pulses, and the remnant resistance is extracted by measuring the current (voltage). High resolution Scanning Transmission Electron Microscopy (HRTEM) with High Angular Annular Dark Field Detector (STEM-HAADF) was performed with a FEI Titan G2 microscope with probe corrector (60-300 keV). Local chemical analysis was performed by Energy Dispersive Spectroscopy (EDS, Oxford Instruments). TEM lamellas

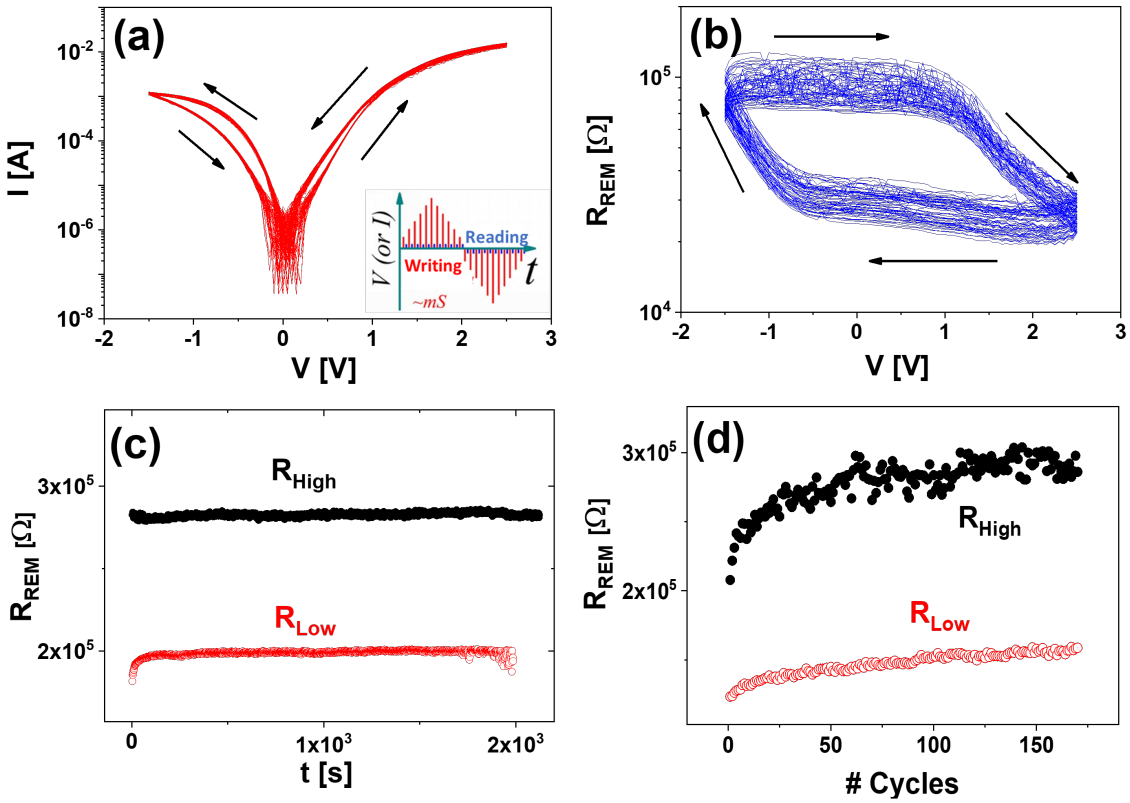

FIG. 1: (a) Dynamic pulsed I–V curve measured on a NSTO/LSMCO/Pt device stimulated with voltage. The arrows indicate the chirality of the curve; (b) Hysteresis switching loop recorded on the same device. The inset in panel (a) sketches the protocol of electrical stimulation; (c) Retention experiments corresponding to the same device, both for R_{LOW} and R_{HIGH} states; (d) Cycle-to-cycle variation test performed on the same device by applying single SET and RESET voltage pulses with opposite polarities

were prepared by Focused Ion Beam (FIB) in a Helios 650 Dual Beam Equipment.

III. RESULTS

The devices were initialized (electroforming process) by applying single pulses of both voltage and current, which produced a drop of the resistance from the virgin state of $\approx 10^5$ Ω to ≈ 80 Ω and ≈ 200 Ω, respectively, as shown in Figure S2.

Figures 1(a) and (b) show dynamic IV curves and HSLs, respectively, recorded on a device stimulated with voltage during 100 cycles. The presence of hysteresis in both cases

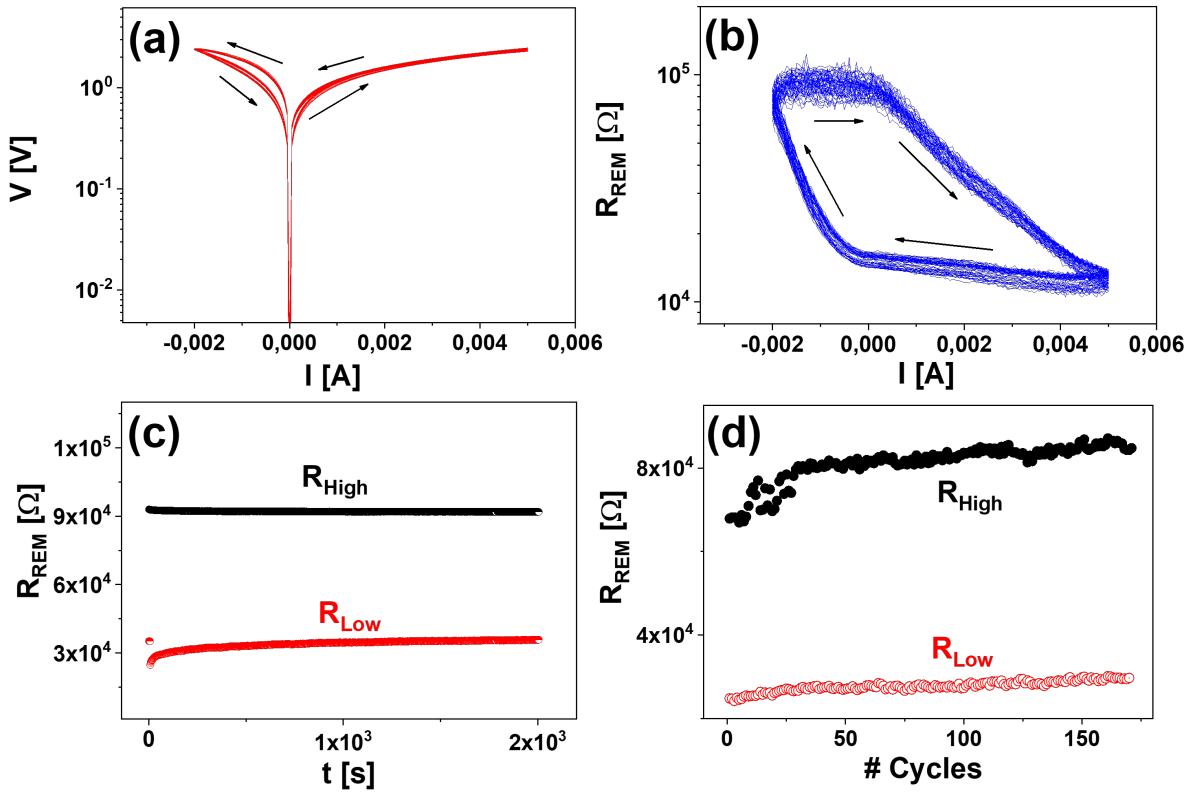

FIG. 2: (a) Dynamic pulsed I–V curve recorded on a NSTO/LSMCO/Pt device stimulated with current. The arrows indicate the chirality of the curve.; (b) Hysteresis switching loop recorded simultaneously with the I–V curve on the same device;(c) Retention experiments recorded on the same device for both R_{LOW} and R_{LOW} states; (d) Cycle-to-cycle variation test measured on the same device.

is a signature of the memristive effect. The SET transition is observed for $\approx$ 2.5 V, while the inverse transition (low to high resistance, RESET) takes place for $\approx$ -1.5 V. The high and low resistance levels are $R_{HIGH} \approx 1x10^5$ Ω and $R_{LOW} \approx 2x10^4$ Ω, respectively, giving an ON-OFF ratio of $\approx$ 5. Figure 1(c) displays retention time experiments for both R_{HIGH} and R_{LOW} up to $2x10^3$ s. Finally, Figure 1(d) shows cycle-to-cycle variation experiments, recorded by applying single pulses of 2.5 V and -1.5 V to switch the device between R_{HIGH} and R_{LOW}. Is is found that both resistance states present a drift towards higher resistance values -which is more pronounced for R_{HIGH} and the first $\approx 10^2$ s after the start of the test- upon cycling-.

Figures 2(a) and (b) show the measured IV curve and HSL on the device stimulated with

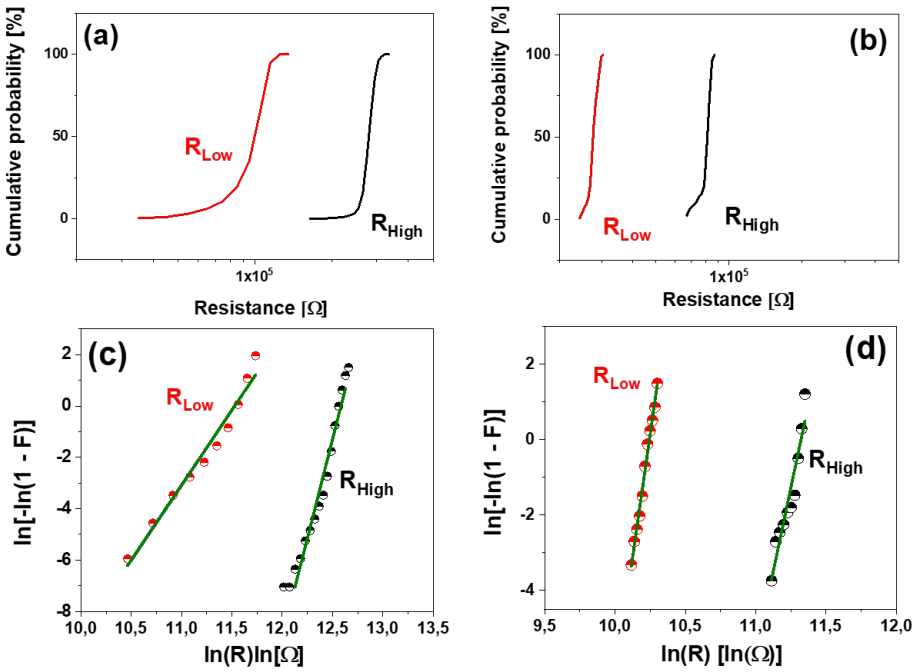

FIG. 3: Cumulative probabilities, obtained from cycle-to-cycle variation tests, for R_{HIGH} and R_{LOW} states and voltage (panel (a)) and current (panel (b)) stimulation; (c), (d) Weibull fittings for R_{HIGH} and R_{LOW} states and voltage (c) and current (d) stimulation. See the main text for details.

current. The SET (RESET) transition is observed for $5x10^{-3}$ A ($-2x10^{-3}$ A). Resistance levels are $R_{HIGH} \approx 10^6$ Ω and $R_{LOW} \approx 10^4$ Ω, respectively, with an ON-OFF ratio of ≈ 100. Figure 2(c) display retention times up to up to $2x10^3$ s. Finally, Figure 2(d) display cycle-to-cycle variation tests recorded after applying single pulses of $5x10^{-3}$ A and $-2x10^{-3}$ A to trigger the SET and RESET transitions, respectively. In this case, the drift of both R_{HIGH} and R_{LOW} upon pulsing is milder that in the case of voltage stimulation. This is also reflected by Figures 3(a) and (b), which show the calculated cumulative probabilities (F) for both R_{HIGH} and R_{LOW} and voltage and current stimulation, respectively. The inspection of this Figure evidences that the R_{HIGH} and R_{LOW} curves corresponding to the current-controlled device are steeper and comprise narrower resistance windows, reflecting a lower cycle-to-cycle variability.

It has been shown [24] that the evolution of both R_{HIGH} and R_{LOW} states upon repeated cycling can be described by a Weibull probability distribution f given by

$$f(R;\lambda,k) = \frac{k}{\lambda}\left(\frac{R}{\lambda}\right)^{k-1} e^{-(R/\lambda)^k} \quad (1)$$

where λ is the scale parameter, k is the shape parameter and R is the resistance. This gives the following expression for the cumulative probability F

$$F(R;\lambda,k) = 1 - e^{-(R/\lambda)^k} \quad (2)$$

which can be linearized as follows

$$\ln(-\ln(1 - F(R;\lambda,k))) = k\ln R - k\ln\lambda \quad (3)$$

Using the experimental values obtained for F, in Figures 3(c) and (d) we have plotted $ln(-\ln(1-F))$ as a function of $ln(R)$, being found a linear behavior -with slopes given by the parameter k- for both R_{HIGH} and R_{LOW}, validating the assumption of cycle-to-cycle variations described by Weibull probability distributions. By performing linear fittings we have extracted values of λ and k for both types of stimulation. For voltage stimulated devices, we obtained, for R_{HIGH}, $\lambda = 2.9x10^5\Omega$ and k = 15.4 and, for R_{LOW}, $\lambda = 1.0x10^5\Omega$ and k = 5.8. For current operated devices we obtained, for R_{HIGH}, $\lambda = 8.2x10^4\Omega$ and k = 17.7 and, for R_{LOW}, $\lambda = 2.8x10^4\Omega$ and k = 26.0. The lower cycle-to-cycle variations of the current stimulated device is reflected in the higher values obtained for k for both resistive states, related to narrower Weibull distributions (the limit case $k \to \infty$ corresponds to a Dirac delta function with no cycle-to-cycle variations).

From the data presented before, it can be concluded that current stimulation seems to produce a more stable memristive behavior. In order to get a better understanding at the nanoscale scenario linked to this behavior, we have performed HRTEM experiments of virgin, stimulated with voltage and stimulated with current devices.

Figure 4(a) shows a low magnification STEM-HAADF image corresponding to a virgin device. LSMCO and Pt thicknesses of $\approx$ 38.5 nm and $\approx$ 29.0 nm are seen. The high resolution image of Figure 4(b) shows the crystalline character of the NSTO substrate together with the amorphous nature of the LSMCO layer. This is confirmed by the Fast Fourier Transforms displayed in Figure S3. Figure 4(c) shows an EDS line-scan that quantifies the cationic composition. It is observed a LSMCO cationic stochiometry consistent with the nominal one (25 % at. for La, Sr, Mn and Co). The oxygen composition was quantified

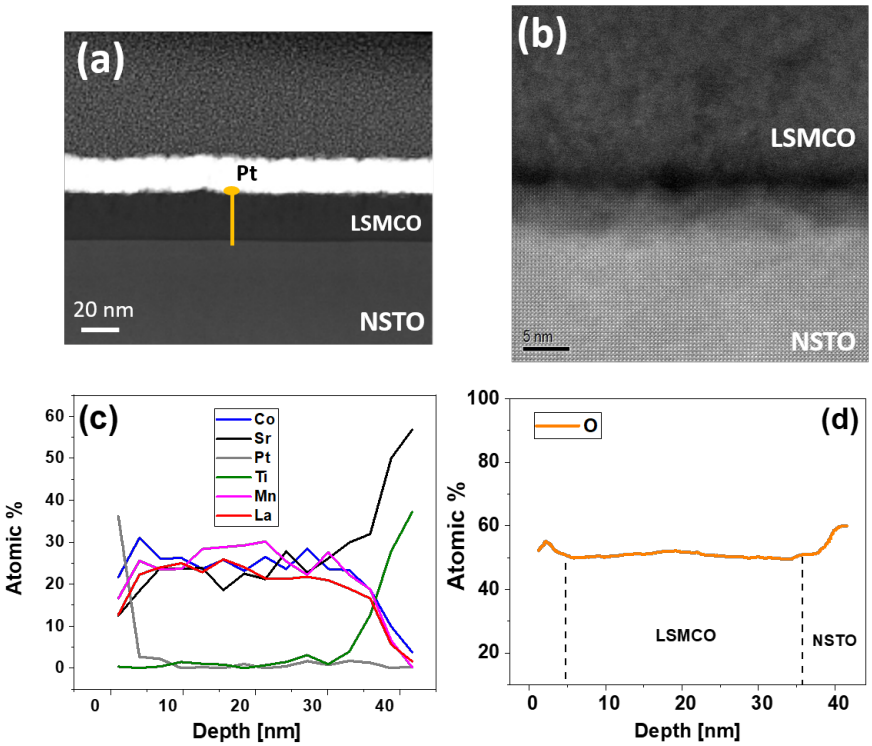

FIG. 4: (a) Low-magnification STEM-HAADF cross-section corresponding to a virgin NSTO/LSMCO/Pt device; (b) High-resolution STEM-HAADF cross section recorded on the same device; (c) EDS line scans quantifying Sr, Ti, Mn, La, and Co cations in a virgin NSTO/LSMCO/Pt device.The scan, indicated in (a) with a yellow line, goes from the LSMCO/Pt interface to the NSTO substrate. (d) EELS oxygen line scan recorded on the same sample.

from the EELS line-scan displayed in Figure 4(d), evidencing some oxygen deficiency ($\approx$ 50 % at.) in relation to the nominal one (60 % at.).

Figure 5(a) shows a low magnification STEM-HAADF cross-section corresponding to a device stressed with voltage. Several changes can be seen; the most important one is related to the observation that the LSMCO layer is splitted in two layers with dissimilar HAADF contrast, indicating that they have different chemical composition. Figure 5(b) shows a high magnification STEM-HAADF image, displaying that the bottom (brighter) layer is crystalline, while the top one (darker) seems to remain amorphous. This is confirmed by the Fast Fourier Transforms shown in Figure S4. In order to obtain further information about the chemistry of these layers, we have performed an EDS line-scan, which is displayed in

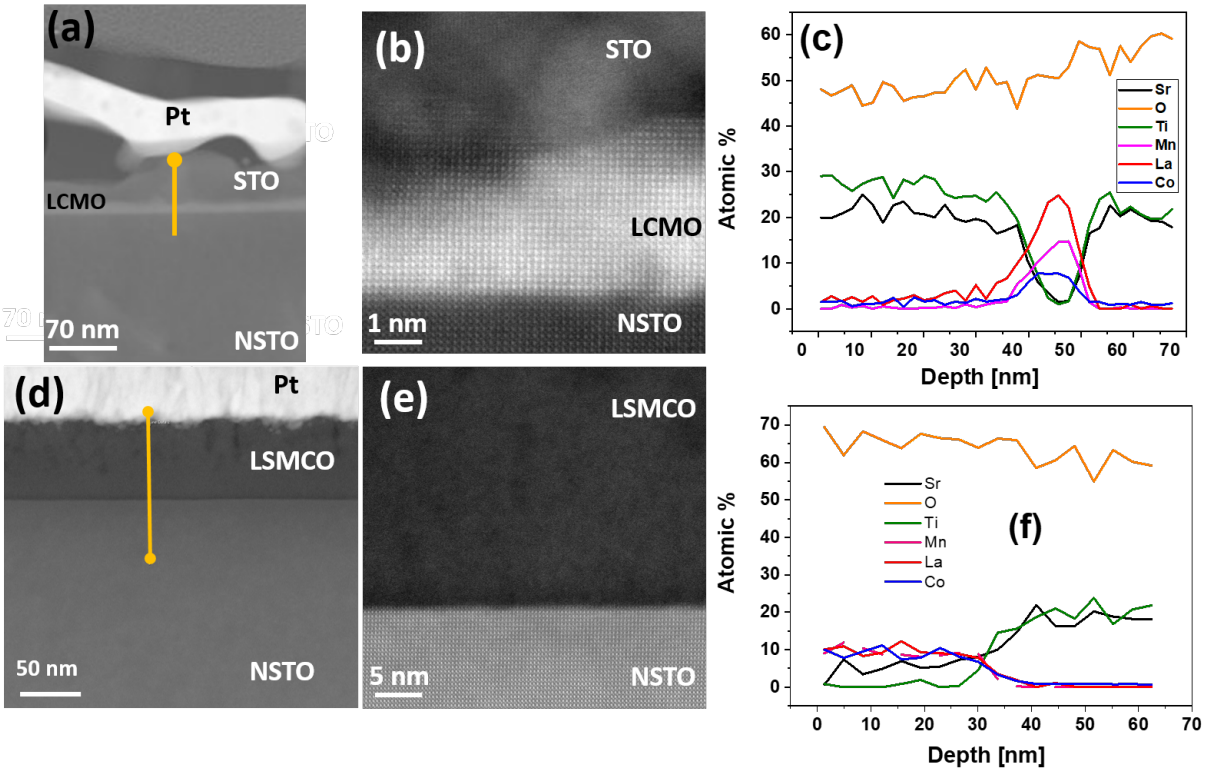

FIG. 5: (a), (d) Low magnification STEM-HAADF cross-sections recorded on NSTO/LSMCO/Pt devices stimulated with voltage and current, respectively(b) and (e) show high-resolution STEM-HAADF cross-sections stimulated with voltage and current; (c); (f) High-resolution STEM-HAADF cross-sections recorded on NSTO/LSMCO/Pt devices stimulated with voltage and current, respectively; (c), (f) EDS line scans quantifying Sr, Ti, Mn, La, Co, and O elements in NSTO/LSMCO/Pt devices stimulated with voltage and current, respectively. As indicated with yellow lines in (a) and (d), the scans start at the LSMCO/Pt the interface and end in the NSTO substrate.

Figure 5(c). It is seen that the top layer consists in $SrTiO_3$ while the bottom one presents a chemical composition consistent with the one of La_2CoMnO_6 perovskite. In consequence, the application of voltage stimulation triggers a strong cationic diffusion that modifies the LSMCO chemistry, probably accelerated by self-heating effects that also induces the (partial) crystallization of the oxide layer, as previously seen in other oxide memristive systems [25].. Figure 5(a) also shows the existence of a meandered top Pt electrode and the presence of "voids" at the Pt/oxide interface, also reflecting the effect of the high temperatures achieved during device operation [26].

Figure 5(d) shows a low magnification STEM-HAADF cross-section corresponding to a device stimulated with current. Despite the presence of some extended defects, appearing with darker contrast and located closer to the top interface with the Pt electrode, the LSMCO layer displays a rather uniform STEM-HAADF brightness, suggesting the absence of cation segregation, unlike the case of the device operated with voltage (recall Figures 5(a)-(c)). The high magnification cross-section of Figure 5(e) confirms this scenario; in addition, this image suggests that the amorphous character of the LSMCO layer is preserved upon stimulation with current. Again, this is in sharp contrast with the voltage operated device, which showed the partial crystallization of the oxide layer upon stimulation with voltage. Finally, the EDS line-scan displayed in Figure 5(f) shows that the nominal cation stochiometry is maintained in the device operated with current, without significant differences with regard the virgin device. The oxygen content, instead, seems to be slightly higher in this device, suggesting some oxygen uptake in the LSMCO layer during the device operation. Oxygen can be obtained from the ambient via a diffusion process through the Pt top electrode grain boundaries [27].

IV. DISCUSSION AND CONCLUSSIONS

The previously presented data indicate substantial differences in the chemistry of the devices operated either with voltage or current. For the case of the device stimulated with voltage, we observed the partial crystallization of the oxide layer together with strong cation difussion that changes the chemistry of the layer. This likely takes place during the device electroforming step and is related to the high temperatures achieved in the device for this type of electrical stimulation. The memristive behavior in this case presents a higher cycle-to-cycle variability. The memristive mechanism can be related to the electromigration of oxygen vacancies between $SrTiO_3$ and La_2CoMnO_6 layers, which are both n-type insulators that locally increase their conductivities in the presence of oxygen vacancies [28, 29].

On the other hand, the device operated with current displayed no significant crystallization process, together with a maintained chemical composition in relation to the pristine device. Lower cycle-to-cycle variations were observed in relation to the voltage operated device. We relate this observations with the self-limited electrical power injection in current controlled mode. The memristive mechanism in this case is likely related to the electromi-

gration of oxygen vacancies between the LSMCO layer (p-type) and the NSTO substrate (n-type), presenting an interface with a rectifying behavior, as shown in Figure S5 (i.e. an n-p diode is formed). Assuming that the number of donors at NSTO ($N_D \approx$ 5x10^{18} [30]) is much lower than the number of acceptors at the LSMCO layer ($N_A \approx 10^{22}$, arising from the $\approx$ 0.5 holes/f.u. related to the substitution of half of the La^{3+} ions by Sr^{2+}), the diode depletion layer W should depend on N_D as W $\propto N_D^{-0.5}$. The injection of oxygen vacancies in the NSTO crystal (achieved with positive voltage) increases N_D and therefore reduces W, lowering in this way the interface resistance.

In summary, our results show that strong cationic segregation can take place in amorphous memristors during electrical operation. The enhanced cationic diffusion occurring in these type of materials is related to their lack of long-range ordering and with the existence of reduced energy barriers for ion movement, together with the absence of extended defects, such as dislocations, that usually hinder ion diffusion. Our results show that the switching of the electrical stimulation from voltage to current allows to significantly reduce chemical changes related to cationic segregation, helping to maintain the device structure and chemistry at the nanoscale and improving the memristive performance by reducing cycle-to-cycle variations. These results could help to the design of more reliable oxide-based memristors, pointing also out the key importance of the type of electrical stimulation that is applied to the devices on key memristive figures such as cycle-to-cycle variations and endurance.

Acknowledgements

We acknowledge support from ANPCyT (PICT2019-02781, PICT2020A-00415) and EU-H2020-RISE project MELON (Grant No. 872631).

Supplementary Material

See Supplementary Material for additional x-ray reflectivity and transmission electron microscopy experiments and electrical measurements.

AUTHOR DECLARATIONS

Conflict of Interest

The authors have no conflicts to disclose.

Data availability

The data that support the findings of this study are available from the corresponding

author upon reasonable request.

---

[1] A. Sawa, Resistive switching in transition metal oxides, Materials Today **11**, 28 (2008).

[2] K. F. A. Zahoor Furqan, Azni Zulkifli Tun Zainal, Resistive random access memory (rram): an overview of materials, switching mechanism, performance, multilevel cell (mlc) storage, modeling, and applications, Nanoscale Research Letters **15**, 1 (2020).

[3] I. K. Schuller, A. Frano, R. C. Dynes, A. Hoffmann, B. Noheda, C. Schuman, A. Sebastian, and J. Shen, Neuromorphic computing: Challenges from quantum materials to emergent connectivity, Applied Physics Letters **120**, 1 (2022).

[4] A. Serb, A. Corna, R. George, A. Khiat, F. Rocchi, M. Reato, M. Maschietto, C. Mayr, G. Indiveri, S. Vassanelli, and T. Prodromakis, Memristive synapses connect brain and silicon spiking neurons, Scientific Reports **10**, 1 (2020).

[5] S.-O. Park, H. Jeong, J. Park, J. Bae, and S. Choi, Experimental demonstration of highly reliable dynamic memristor for artificial neuron and neuromorphic computing, Nature Communications **13**, 1 (2022).

[6] L. Bégon-Lours, M. Halter, F. M. Puglisi, L. Benatti, D. F. Falcone, Y. Popoff, D. Dávila Pineda, M. Sousa, and B. J. Offrein, Scaled, ferroelectric memristive synapse for back-end-of-line integration with neuromorphic hardware, Advanced Electronic Materials **8**, 1 (2022).

[7] F. Gunkel, D. V. Christensen, Y. Z. Chen, and N. Pryds, Oxygen vacancies: The (in)visible friend of oxide electronics, Applied Physics Letters **116**, 1 (2020).

[8] D.-H. Kwon, K. M. Kim, J. H. Jang, J. M. Jeon, M. H. Lee, G. H. Kim, X.-S. Li, G.-S. Park, B. Lee, S. Han, M. Kim, and C. S. Hwang, Atomic structure of conducting nanofilaments in tio2 resistive switching memory, Applied Physics Letters **5**, 148 (2010).

[9] A. Herpers, C. Lenser, C. Park, F. Offi, F. Borgatti, G. Panaccione, S. Menzel, R. Waser, and R. Dittmann, Spectroscopic proof of the correlation between redox-state and charge-carrier transport at the interface of resistively switching ti/pcmo devices, Advanced Materials **26**, 2730 (2014).

[10] K. Fujiwara, T. Nemoto, M. J. Rozenberg, Y. Nakamura, and H. Takagi, Resistance switching and formation of a conductive bridge in metal/binary oxide/metal structure for memory

devices, Japanese Journal of Applied Physics **47**, 6266 (2008).

[11] I. Valov, R. Waser, J. R. Jameson, and M. N. Kozicki, Electrochemical metallization memories -fundamentals, applications, prospects, Nanotechnology **22**, 1 (2011).

[12] C. Lenser, A. Koehl, I. Slipukhina, H. Du, M. Patt, V. Feyer, C. M. Schneider, M. Lezaic, R. Waser, and R. Dittmann, Formation and movement of cationic defects during forming and resistive switching in srtio3 thin film devices, Advanced Functional Materials **25**, 6360 (2015).

[13] W. Lee, S. Yoo, K. J. Yoon, I. W. Yeu, H. J. Chang, J.-H. Choi, S. Hoffmann-Eifert, R. Waser, and C. S. Hwang, Resistance switching behavior of atomic layer deposited srtio3 film through possible formation of sr2ti6o13 or sr1ti11o20 phases, Scientific Reports **6**, 20550 (2016).

[14] G. Di Martino, A. Demetriadou, W. Li, D. Kos, B. Zhu, X. Wang, B. de Nijs, H. Wang, J. MacManus-Driscoll, and J. J. Baumberg, Real-time in situ optical tracking of oxygen vacancy migration in memristors, Nature Electronics **3**, 1 (2020).

[15] W. R. Acevedo, D. Rubi, J. Lecourt, U. Lüders, F. Gomez-Marlasca, P. Granell, F. Golmar, and P. Levy, Manganite-based three level memristive devices with self-healing capability, Physics Letters A **380**, 2870 (2016).

[16] W. Román Acevedo, C. Acha, M. J. Sánchez, P. Levy, and D. Rubi, Origin of multistate resistive switching in ti/manganite/siox/si heterostructures, Applied Physics Letters **110**, 053501 (2017).

[17] A. Aguadero, H. Falcon, J. M. Campos-Martin, S. M. Al-Zahrani, J. L. G. Fierro, and J. A. Alonso, An oxygen-deficient perovskite as selective catalyst in the oxidation of alkyl benzenes, Angewandte Chemie International Edition **50**, 6557 (2011).

[18] W. Román Acevedo, C. A. M. van den Bosch, M. H. Aguirre, C. Acha, A. Cavallaro, C. Ferreyra, M. J. Sánchez, L. Patrone, A. Aguadero, and D. Rubi, Large memcapacitance and memristance at nb:srtio3/la0.5sr0.5mn0.5co0.5o3- topotactic redox interface, Applied Physics Letters **116**, 063502 (2020).

[19] W. Román Acevedo, M. H. Aguirre, C. Ferreyra, M. J. Sánchez, M. Rengifo, C. A. M. van den Bosch, A. Aguadero, B. Noheda, and D. Rubi, Optimization of the multi-mem response of topotactic redox La1/2Sr1/2Mn1/2Co1/2O3x, APL Materials **10**, 011111 (2022).

[20] W. R. Acevedo, M. H. Aguirre, B. Noheda, and D. Rubi, Multi-mem behavior at reduced voltages in $la_{1/2}sr_{1/2}mn_{1/2}co_{1/2}o_{3-x}$ perovskite modified with sm:ceo_2, arxiv.org/abs/2404.14231 (2024).

[21] C. A. M. van den Bosch, A. Cavallaro, R. Moreno, G. Cibin, G. Kerherve, J. M. Caicedo, T. K. Lippert, M. Doebeli, J. Santiso, S. J. Skinner, and A. Aguadero, Revealing strain effects on the chemical composition of perovskite oxide thin films surface, bulk, and interfaces, Advanced Materials Interfaces **7**, 1 (2020).

[22] D. Rubi, F. Tesler, I. Alposta, A. Kalstein, N. Ghenzi, F. Gomez-Marlasca, M. Rozenberg, and P. Levy, Two resistive switching regimes in thin film manganite memory devices on silicon, Applied Physics Letters **103**, 163506 (2013).

[23] M. J. Rozenberg, M. J. Sánchez, R. Weht, C. Acha, F. Gomez-Marlasca, and P. Levy, Mechanism for bipolar resistive switching in transition-metal oxides, Phys. Rev. B **81**, 115101 (2010).

[24] J. Debanjan, S. Subhranu, R. Sourav, L. Y. Feng, and S. Maikap, Observation of resistive switching memory by reducing device size in a new cr/crox/tiox/tin structure, Nano-Micro Letters **7**, 392 (2022).

[25] R. L. Martir, M. J. Sánchez, M. Aguirre, W. Quiñonez, C. Ferreyra, C. Acha, J. Lecourt, U. Lüders, and D. Rubi, Oxygen vacancy dynamics in pt/tiox/taoy/pt memristors: exchange with the environment and internal electromigration, Nanotechnology **34**, 1 (2022).

[26] E. Yalon, S. Cohen, A. Gavrilov, and D. Ritter, Evaluation of the local temperature of conductive filaments in resistive switching materials, Nanotechnology **23**, 465201 (2012).

[27] A. F. Zurhelle, W. Stehling, R. Waser, R. A. De Souza, and S. Menzel, Oxygen diffusion in platinum electrodes: A molecular dynamics study of the role of extended defects, Advanced Materials Interfaces **9**, 2101257 (2022).

[28] R. Li, C. Zhang, J. Liu, J. Zhou, and L. Xu, A review on the electrical properties of doped srtio3 as anode materials for solid oxide fuel cells, Materials Research Express **6**, 1 (2019).

[29] F. N. Sayed, S. N. Achary, S. Deshpande, B. Rajeswari, R. M. Kadam, S. Dwebedi, A. K. Nigam, and A. K. Tyagi, Role of annealing atmosphere on structure, dielectric and magnetic properties of la2comno6 and la2mgmno6, Materials Research Express **640**, 1907 (2014).

[30] K. Ozdogan, M. Upadhyay Kahaly, S. R. Sarath Kumar, H. N. Alshareef, and U. Schwingenschlögl, Enhanced carrier density in nb-doped srtio3 thermoelectrics, Journal of Applied Physics **111**, 1 (2012).